Am J Cancer Res 2024;14(10):4855-4867
www.ajcr.us /ISSN:2156-6976/ajcr0159132

Original Article

Gadolinium-ethoxybenzyl-diethylenetriamine pentaacetic acid-enhanced MRI improves diagnosis and efficacy evaluation of early-stage hepatocellular carcinoma

Ya-Yun Wang[1,2*], Jing Zhang[3*], Xiong Zhuang[1,2], Qiu-Yan Jin[3], Liang-Qing Liu[1,2]

[1]Department of Imaging, Wujin Clinical College of Xuzhou Medical University, Changzhou 213002, Jiangsu, China; [2]Jiangsu Key Laboratory of Encephalopathy Bioinformatics, Xuzhou 221004, Jiangsu, China; [3]Department of Imaging, The Third People's Hospital of Changzhou, Changzhou 213000, Jiangsu, China. [*]Equal contributors.

Received July 11, 2024; Accepted October 13, 2024; Epub October 15, 2024; Published October 30, 2024

Abstract: Objective: To investigate the use of hepatocyte-specific contrast agent Gadolinium-ethoxybenzyl-diethylenetriamine pentaacetic acid-enhanced magnetic resonance imaging (EOB-MRI) in the diagnosis and efficacy evaluation of patients with early-stage hepatocellular carcinoma. Methods: A retrospective clinical study was conducted on 157 patients diagnosed with stage Ia-Ib liver cancer. Of these, 100 patients underwent preoperative EOB-MRI, while 57 patients underwent contrast-enhanced computerized tomography (CECT). The study compared the accuracy, sensitivity, and specificity of these two imaging modalities in diagnosing early-stage hepatocellular carcinoma. In the EOB-MRI group, 100 patients underwent radiofrequency ablation or interventional procedures, and imaging data were collected post-scan. The following arterial and hepatobiliary phase enhancement features were analyzed: length-diameter difference (LDD), signal intensity ratio of metastases to liver parenchyma (RatioM/L), relative signal intensity difference (RSID), normalized relative enhancement (NRE), contrast-to-noise ratio (CNR), and apparent diffusion coefficient (ADC) values. Based on treatment outcomes, patients were categorized into high and low response rate groups, and the imaging parameters between these two groups were compared. Univariate and multivariate analyses were performed to evaluate the significance of these parameters in predicting patient outcomes. Results: The accuracy of lesion detection by EOB-MRI was 97.4%, significantly higher than that of CECT (80.0%) ($P < 0.05$). The area under the curve (AUC) for the EOB-MRI group was 0.923 (95% CI: 0.784-1.000), with a sensitivity of 97.4% and a specificity of 83.3%. In comparison, the AUC for the CECT group was 0.712 (95% CI: 0.582-0.843), with a sensitivity of 77.2% and a specificity of 65.2%. The median response rate of patients with early-stage hepatocellular carcinoma to systemic therapy was 60% (range: 36%-81%). Using 60% as the cut-off value, patients were divided into a high response rate group (n = 53) and a low response rate group (n = 47). Univariate and multivariate logistic regression analyses of the EOB-MRI parameters in both groups identified ADC and NRE as independent predictors for assessing the treatment efficacy of early-stage hepatocellular carcinoma. Conclusion: EOB-MRI is effective for both the diagnosis and evaluation of treatment efficacy in early-stage hepatocellular carcinoma.

Keywords: Gadolinium-ethoxybenzyl-diethylenetriamine pentaacetic acid (Gd-EOB-DTPA), magnetic resonance imaging (MRI), hepatocellular carcinoma, diagnose, treatment response rate

Introduction

Primary hepatocellular carcinoma is a malignant tumor with a widespread global distribution, ranking as the fourth most common and the second most lethal cancer in China [1-3]. With 410,000 new cases and 391,000 deaths annually, China accounts for 45.3% and 47.1% of the global burden of hepatocellular carcinoma, respectively [4, 5]. Currently, the median overall survival of hepatocellular carcinoma patients in China is just 23 months, with a 5-year survival rate of less than 14.1% [6]. Importantly, studies have shown that when hepatocellular carcinoma is diagnosed at an early stage - such as Stage 0 or Stage A of the Barcelona Clinic Liver Cancer (BCLC) staging system - the 5-year survival rate can reach up to 86.2% [7, 8]. At these stages, the tumor is typically small, with no vascular invasion or distant metastasis, and patients generally have preserved liver function and good physical status,

https://doi.org/10.62347/WYNK6968

which may positively impact treatment efficacy and prognosis following systemic therapy. This underscores the strong correlation between early diagnosis and improved long-term survival outcomes in hepatocellular carcinoma patients [9]. However, in mainland China, the early diagnosis rate for hepatocellular carcinoma remains below 30%. Therefore, developing an efficient and accurate method for early-stage diagnosis is of critical importance.

In current clinical practice, imaging plays a crucial role in the diagnosis and treatment of hepatocellular carcinoma. Common imaging modalities include contrast-enhanced computerized tomography (CECT), magnetic resonance imaging (MRI), ultrasound, and positron emission tomography-computed tomography (PET-CT). Among these, CECT and MRI are the preferred follow-up options when abnormalities are detected via ultrasound or test markers [10, 11]. CECT is a tomographic imaging technique that utilizes X-rays and computer technology. By injecting a contrast agent, it enhances image clarity, allowing for a more detailed view of vascular and tissue structures in organs like the liver. CECT's ability to perform sequential scans at different time points to capture the dynamic distribution of contrast agents in the liver makes it especially useful for emergency and rapid diagnoses [12, 13]. However, CECT has notable limitations, particularly in detecting lesions smaller than 1 cm, where its sensitivity is inferior to other techniques, such as Gadolinium-ethoxybenzyl-diethylenetriamine pentaacetic acid-enhanced magnetic resonance imaging (EOB-MRI).

Gadolinium-ethoxybenzyl-diethylenetriamine pentaacetic acid (Gd-EOB-DTPA) is a novel liver-specific contrast agent. In addition to the properties of conventional extracellular interstitial contrast agents, Gd-EOB-DTPA can be absorbed by hepatocytes, providing a dual contrast function [14-16]. In the diagnosis of hepatocellular carcinoma, its typical imaging feature is dynamic enhancement characterized by "fast in, fast out". Specifically, during the arterial phase of an EOB-MRI dynamic enhancement scan, the tumor shows non-circumferential rapid enhancement, while in the portal or delayed phases, the lesion quickly loses contrast, displaying lower density or signal intensity compared to normal liver parenchyma, particularly during the hepatobiliary phase. These imaging characteristics, especially the low signal in the hepatobiliary phase, have significantly improved the detection rate of hepatocellular carcinoma, particularly for small or microscopic lesions [17-19]. Given these advantages, EOB-MRI was recommended as a first-line diagnostic tool for hepatocellular carcinoma in the updated 2017 *Clinical Management Practice for Hepatocellular Carcinoma in the Asia-Pacific Region* and the 2018 *Korean Guidelines for Hepatocellular Carcinoma Management Practice* [20, 21]. Therefore, EOB-MRI offers substantial benefits for both the diagnosis and differential diagnosis of hepatobiliary diseases.

However, current research has yet to fully clarify the role of EOB-MRI in the diagnosis, treatment efficacy evaluation, and prognosis of patients with early-stage hepatocellular carcinoma. To address this gap, our study retrospectively analyzed 157 patients with early-stage hepatocellular carcinoma. The objective was to assess the diagnostic accuracy of EOB-MRI in these patients and to further investigate the value of EOB-MRI-related parameters in evaluating treatment efficacy in early-stage hepatocellular carcinoma.

Data and methods

General information

We retrospectively collected data from 157 patients who underwent EOB-MRI or CECT following a preliminary diagnosis of focal liver lesions at Wujin Clinical College of Xuzhou Medical University, Jiangsu, and the Third People's Hospital of Changzhou, between January 2021 and March 2024. Patients were divided into two groups based on the imaging modality used: the EOB-MRI group (n = 100) and the CECT group (n = 57). The basic study flow is shown in **Figure 1**.

Inclusion criteria: 1) patients aged between 18 and 75 years; 2) diagnosed with primary hepatocellular carcinoma through clinical or biopsy-based pathological examination; 3) classified as China Liver Cancer Staging (CNLC) stage Ia or Ib: single tumor ≤ 5 cm in diameter, or multiple tumors (up to 3) with a diameter > 5 cm, without vascular invasion or extrahepatic metastasis [22, 23]; 4) no contraindications to EOB-MRI or CECT; 5) underwent EOB-MRI after treatment with radiofrequency ablation.

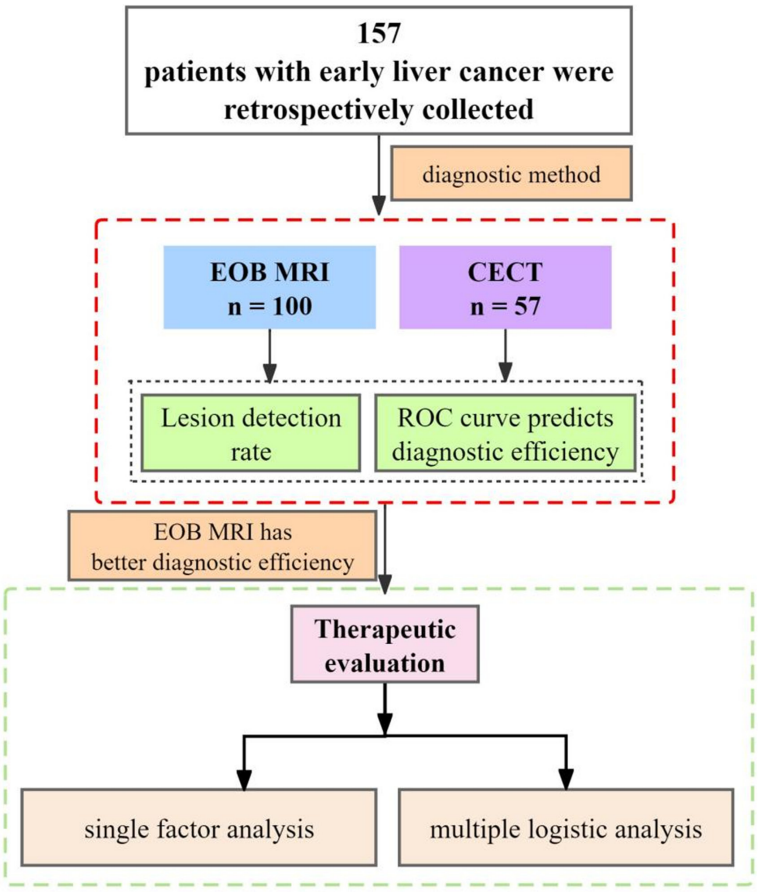

Figure 1. Basic research process. EOB-MRI: Gadolinium-ethoxybenzyl-diethylenetriamine pentaacetic acid-enhanced magnetic resonance imaging; CECT: contrast-enhanced computerized tomography; ROC: receiver operator characteristic curve.

Exclusion criteria: 1) poor image quality or incomplete follow-up data; 2) diffuse hepatic lesions; 3) non-initial hepatic therapeutic surgery; 4) hepatic malignancy combined with cancerous or portal vein thrombosis in major branches; 5) severe cardiac, cerebral, renal, or circulatory diseases, or primary malignancies from other systems.

This study was approved by the Ethics Committee of Wujin Clinical College of Xuzhou Medical University, Jiangsu.

Gd-EOB-DTPA MRI examination

A total of 100 patients underwent EOB-MRI, with fasting for 4-6 hours prior to the examination and resting for 15-30 minutes before scanning. EOB-MRI examination protocol: 1) A 0.1 ml/kg dose of Gd-EOB-DTPA contrast agent was manually injected at a flow rate of 2 ml/s, followed by flushing the syringe with at least 2 ml of saline. 2) The scanning sequences included coronal T2-weighted imaging (T2WI), axial T1-weighted imaging (T1WI) with anteroposterior phase, T2WI fat suppression, diffusion-weighted imaging (DWI) (b-values of 50 and 800), and dynamic contrast-enhanced scans in the arterial phase (30 s), portal venous phase (60 s, 120 s), and transitional phases (5, 10, and 15 min). The hepatobiliary phase was captured at 20 minutes post-injection.

Image analysis: Observations were made using the Picture Archiving and Communications System (PACS). The images were independently analyzed by two abdominal imaging specialists with 5 and 7 years of experience, respectively, who were blinded to the pathological results. Judgment criteria: Hepatocellular carcinoma was diagnosed when the lesion exhibited the following characteristics: slightly high signal intensity on T2-weighted (T2WI) images; slightly low signal intensity on T1-weighted (T1WI) images; high signal on diffusion-weighted images (DWI) with no signal attenuation as the b-value increased; rapid arterial phase enhancement; ring or delayed enhancement in the portal or equilibrium phases; low signal in the hepatobiliary phase. The number, location, size, and enhancement patterns of the tumors were determined based on multiple sequences of DWI images with different b-values (50 and 800), which also helped in differentiating hepatocellular carcinoma from other intrahepatic lesions.

Gd-EOB-DTPA MRI parameters

All patients who underwent radiofrequency ablation or intervention were categorized into two groups based on their treatment response: a high response rate group and a low response

rate group. The median response rate to systemic treatment served as the cut-off value. Post-treatment, 100 patients underwent a follow-up EOB-MRI, with the interval between radiofrequency ablation or intervention and the post-procedure examination being at least 1 month. The same imaging protocol used in the previous section was followed. Specifically, images from the late arterial phase and the 20-minute hepatobiliary phase were selected for analysis.

Image analysis and data measurement: (1) Qualitative assessment of enhancement characteristics: 1) Arterial phase enhancement: tumors were assessed for either circular or non-circular enhancement patterns. 2) Hepatobiliary phase enhancement: lesions were classified based on whether they showed target-like or non-target-like enhancement patterns. In case of disagreements, the supervising physician would lead a discussion, and consensus would be used for subsequent analysis. (2) Quantitative measurement of lesion signals: 1) Arterial and hepatobiliary phases: the largest cross-section of the lesion was selected, and the longest diameter of the tumor was measured. For tumors with ring-shaped enhancement in the arterial phase, the measurement included the longest diameter, incorporating the enhancement ring. 2) Apparent diffusion coefficient (ADC) image: the largest cross-section of the lesion was selected, and the ADC value was measured. The region of interest (ROI) encompassed as much of the lesion as possible. 3) Signal intensities of lesions and surrounding liver parenchyma (SIM0), parenchyma (SIL0), and renal cortex (SIR0) on T1-weighted pre-contrast images were measured. 4) In the hepatobiliary stage, signal intensities of lesions (SIL20), peripheral liver parenchyma (SIL20), renal cortex (SIR20), and background noise (SDN20) on T1-weighted hepatobiliary phase images were measured.

The signal intensity of the lesion was measured from the largest cross-sectional area of the tumor, ensuring that the ROI encompassed the entire tumor as much as possible. For liver parenchyma, measurements were taken while avoiding blood vessels and bile ducts. Four ROIs, each measuring 1 cm in size, were delineated and averaged. Renal cortex measurements were performed at the level of the renal hilum, with eight ROIs of 3-4 mm in size drawn and averaged. Background noise measurements were obtained by placing eight 1-2 cm ROIs in the four quadrants (upper right, lower right, upper left, and lower left) of the image, and the average of these measurements was used. Quantitative parameters were measured by two physicians independently, and the average of their measurements was taken as the data for subsequent analysis.

The following parameters were calculated using the measured data: (1) the difference of long diameter between arterial and hepatobiliary phase was calculated, with a difference of ≥ 2 mm being considered indicative of enhancement of the liver parenchyma around the lesion; (2) signal intensity ratio of metastases to liver parenchyma (RatioM/L) = SIM20/SIL20; (3) relative signal intensity difference (RSID) = SIL20 - SIM20; (4) normalized relative enhancement (NRE) = (SIM20/SIR20 - SIM0/SIR0) × SIR0/SIM0 × 100%; (5) contrast-to-noise ratio (CNR) = (SIM20 - SIL20)/SDN20.

CECT check

A total of 57 patients underwent CECT. The patients were positioned supine during the scan, which was performed using either a Siemens dual-source spiral CT or a GE 64-slice spiral CT. The scanning range covered from the top of the diaphragm to the lower edge of the liver. Routine plain scans followed by a three-phase enhanced scan were performed. After the plain scan, a non-ionic iodine-containing contrast agent (iohexol, 300 mg/ml) was injected intravenously at a dose of 2.5-3.0 ml/kg using a high-pressure syringe. The injection was administered at a flow rate of 3 ml/s. Images were collected at three time points following contrast injection: arterial phase at 30 seconds, portal vein phase at 60 seconds, and equilibrium phase at 120 seconds. The scanning parameters were as follows: scanning voltage of 120 kV, scanning current of 280 mA, rotation speed of 0.5 seconds per rotation, and pitch of 1.375:1. After the scan, the images were transmitted to a post-processing workstation for reconstruction. Coronal and sagittal reconstructions of the portal venous phase were selected for analysis.

Image analysis: The analysis method was the same as that used for Gd-EOB-DTPA MRI.

Diagnostic criteria included single or multiple lesions with unclear boundaries, solid or cystic-solid nodules, slightly low or equal density on plain scan, and a certain degree of enhancement on the enhanced scan.

Pathological examination

Radiofrequency ablation or intervention was performed to treat 157 patients with early-stage hepatocellular carcinoma, involving a total of 311 lesions (196 lesions in the EOB-MRI group and 115 lesions in the CECT group). Histologic examination, puncture, and other pathological findings were used as the gold standard for diagnosis.

Evaluation of Gd-EOB-DTPA MRI and CECT in early diagnosis of hepatocellular carcinoma

The detection rates of EOB-MRI and CECT in diagnosing early-stage hepatocellular carcinoma were compared. Receiver operating characteristic (ROC) curves were plotted to calculate the sensitivity and specificity of each imaging modality.

Evaluation of treatment response rate

All 100 patients who underwent Gd-EOB-DTPA MRI and received radiofrequency ablation or intervention were followed up for 3 months to observe the treatment response. The original tissue specimens of these 100 patients with early-stage hepatocellular carcinoma were independently reviewed by two pathologists, who were blinded to the imaging findings. Hematoxylin-eosin (HE) staining was used to observe the ratio of necrotic and fibrotic areas to residual tumor cells microscopically. The mean diagnostic results from both pathologists were taken as the final response rate, with the response quantified as a percentage. This percentage was then used to calculate the average response rate for the lesions in each patient. Based on the median response rate, patients were categorized into high and low response rate groups.

Statistical analysis

SPSS 23.0 was used for data analysis. Quantitative parameters were expressed as mean ± standard deviation (M ± SD), and qualitative parameters were expressed as frequency (n [%]). In the univariate analysis, the χ^2 test was used to analyze qualitative parameters, the independent samples t-test was used for quantitative parameters, and binary logistic regression was employed for multifactorial analysis. A *P*-value of < 0.05 was considered statistically significant.

Results

General information

The age, body mass index, history of hypertension, history of diabetes, disease duration, pathological type, focal mass type, liver function grade, abdominal effusion, albumin level, total bilirubin level, and alpha-fetoprotein level of patients in the EOB-MRI group and the CECT group were similar (**Table 1**).

Comparison of diagnostic results

Detection of lesions: Using histologic examination, puncture, and other pathological findings as the gold standard, the 100 patients who underwent EOB-MRI had a total of 196 lesions, with 91 lesions measuring < 1 cm and 106 lesions measuring ≥ 1 cm. The 57 patients who underwent CECT had a total of 115 lesions, with 55 lesions measuring < 1 cm and 60 lesions measuring ≥ 1 cm.

(1) In the EOB-MRI group, 86 lesions measuring < 1 cm were detected, with a detection rate of 94.5%; 105 lesions measuring ≥ 1 cm were detected, with a detection rate of 99.1%; and the overall detection accuracy was 97.4%. (2) In the CECT group, 40 lesions measuring < 1 cm were detected, with a detection rate of 72.7%; 52 lesions measuring ≥ 1 cm were detected, with a detection rate of 86.7%; and the total detection accuracy was 80.0%. When comparing the detection accuracy between the two groups, the EOB-MRI group demonstrated better detection accuracy (97.4% vs. 80.0%, $P < 0.001$) (**Figure 2**). Imaging examples of lesion detection in both groups are shown in **Figure 3**.

Prediction efficiency evaluated by ROC curves: As shown in **Figure 4**, the diameters of lesions detected by EOB-MRI and CECT were statistically comparable for lesions < 1 cm and ≥ 1 cm. The average diameter of < 1 cm lesions was

Table 1. General information [$\bar{x}$ ± s, n (%)]

Projects	*n*	EOB-MRI (*n* = 100)	CECT (*n* = 57)	χ^2/t	*P*
Age		48.2 ± 16.6	46.4 ± 16.0	0.643	0.521
BMI (kg/m^2)		24.1 ± 3.4	23.5 ± 3.9	0.877	0.382
Hypertension history [*n* (%)]				0.178	0.673
Yes	36 (22.9)	24 (24.0)	12 (21.1)		
No	121 (77.1)	76 (76.0)	45 (78.9)		
History of diabetes [*n* (%)]				0.039	0.844
Yes	26 (16.6)	17 (17.0)	9 (15.8)		
No	131 (83.4)	83 (83.0)	48 (84.2)		
Duration of disease (month)		7.6 ± 1.5	7.6 ± 2.6	-0.164	0.870
Pathological classification [*n* (%)]				0.431	0.511
Nodular type	115 (73.2)	75 (75.0)	40 (70.2)		
Block type	42 (26.8)	25 (25.0)	17 (29.8)		
Liver function classification				0.223	0.637
A	87 (55.4)	54 (54.0)	33 (57.9)		
B	70 (44.6)	46 (46.0)	24 (42.1)		
Seroperitoneum				1.254	0.263
Yes	5 (3.2)	2 (2.0)	3 (5.3)		
No	152 (96.8)	98 (98.0)	54 (94.7)		
Albumin (g/dL)		3.9 ± 1.1	4.0 ± 1.2	-0.550	0.583
Total bilirubin (mg/dL)		0.9 ± 0.5	1.0 ± 0.5	-1.623	0.107
Alpha fetoprotein (ng/dL)		7.0 ± 1.1	7.2 ± 1.2	-0.926	0.356

Note: EOB-MRI: Gadolinium-ethoxybenzyl-diethylenetriamine pentaacetic acid-enhanced magnetic resonance imaging; CECT: contrast-enhanced computerized tomography; BMI: body mass index.

A

Confusion matrix		EOB-MRI results		
		< 1cm	≥ 1cm	Total
Case outcome	< 1cm	86	5	91
	≥ 1cm	1	105	106
	Total	87	110	

B

Confusion matrix		CECT results		
		< 1cm	≥ 1cm	Total
Case outcome	< 1cm	40	15	55
	≥ 1cm	8	52	60
	Total	48	67	

Figure 2. Two groups of confusion matrices. A: Gadolinium-ethoxybenzyl-diethylenetriamine pentaacetic acid-enhanced magnetic resonance imaging (EOB-MRI); B: Contrast-enhanced computerized tomography (CECT).

0.6 ± 0.2 cm for EOB-MRI and 0.6 ± 0.3 cm for CECT, while for ≥ 1 cm lesions, the average diameter was 2.5 ± 0.9 cm for EOB-MRI and 2.4 ± 0.8 cm for CECT, indicating no significant

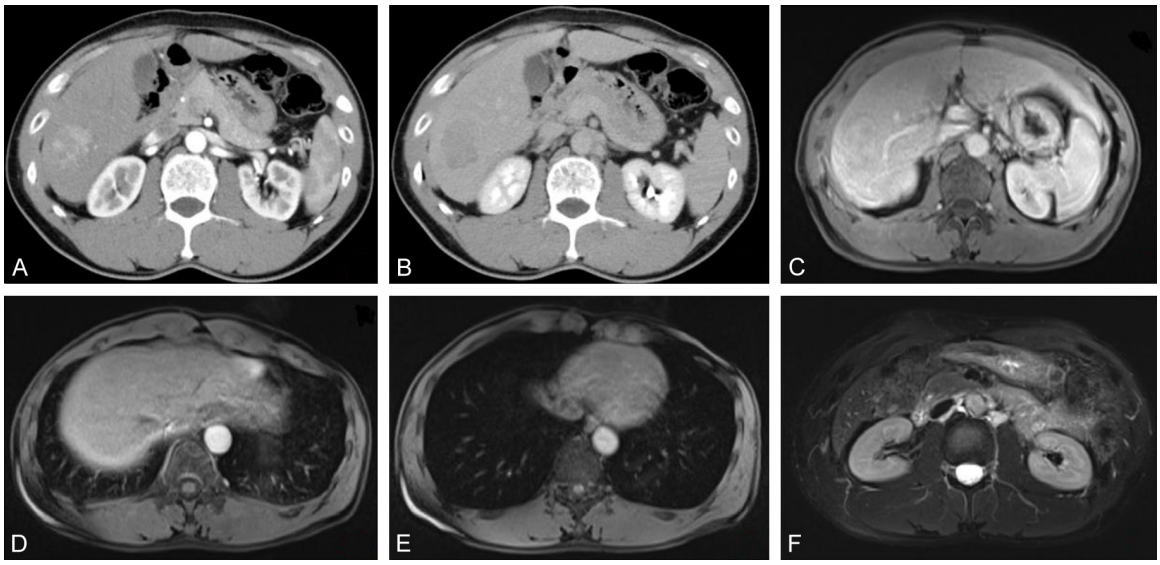

Figure 3. Case image of a 57-year-old male. A: CT-enhanced arterial stage; B: CT-enhanced venous stage; C: EOB-MRI early arterial stage; D: EOB-MRI late arterial stage lesion with mild enhancement; E: EOB-MRI venous stage lesion with mild enhancement; F: EOB-MRI hepatobiliary stage lesion with slightly high signal. EOB-MRI: Gadolinium-ethoxybenzyl-diethylenetriamine pentaacetic acid-enhanced magnetic resonance imaging; CECT: contrast-enhanced computerized tomography.

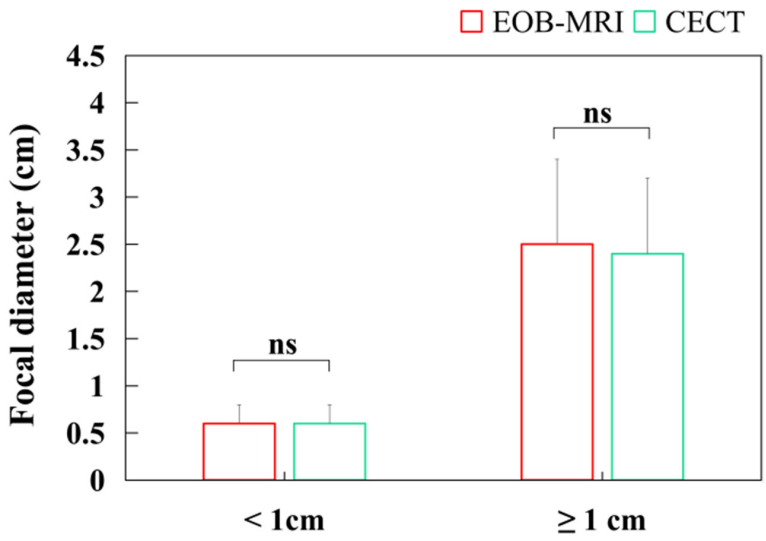

Figure 4. Lesion diameters of the two groups. EOB-MRI: Gadolinium-ethoxybenzyl-diethylenetriamine pentaacetic acid-enhanced magnetic resonance imaging; CECT: contrast-enhanced computerized tomography.

difference between the two groups. The ROC curves for lesion diameter detection in both groups are shown in **Figure 5**. In the EOB-MRI group, the area under the curve (AUC) was 0.923 (95% CI: 0.784-1.000), with a sensitivity of 97.4%, a specificity of 83.3%, and a maximal Youden index of 0.807. In the CECT group, the AUC was 0.712 (95% CI: 0.582-0.843), with a sensitivity of 77.2%, a specificity of 65.2%, and a maximal Youden index of 0.424.

Evaluation of the efficacy of EOB-MRI on early-stage hepatocellular carcinoma

As shown in **Figure 5**, compared with CECT, EOB-MRI demonstrated a higher lesion detection rate and superior diagnostic efficacy in patients with early-stage hepatocellular carcinoma. Based on these findings, the study further explored the efficacy of EOB-MRI parameters in evaluating the treatment outcomes of early-stage hepatocellular carcinoma.

The mean response rate of each lesion to systemic therapy in patients with early-stage hepatocellular carcinoma ranged from 20% to 100%, with a median response rate of 60% (range: 36%, 81%). Based on this cut-off value of 60%, the patients were divided into a high-response-rate group (n = 53) and a low-response-rate group (n = 47).

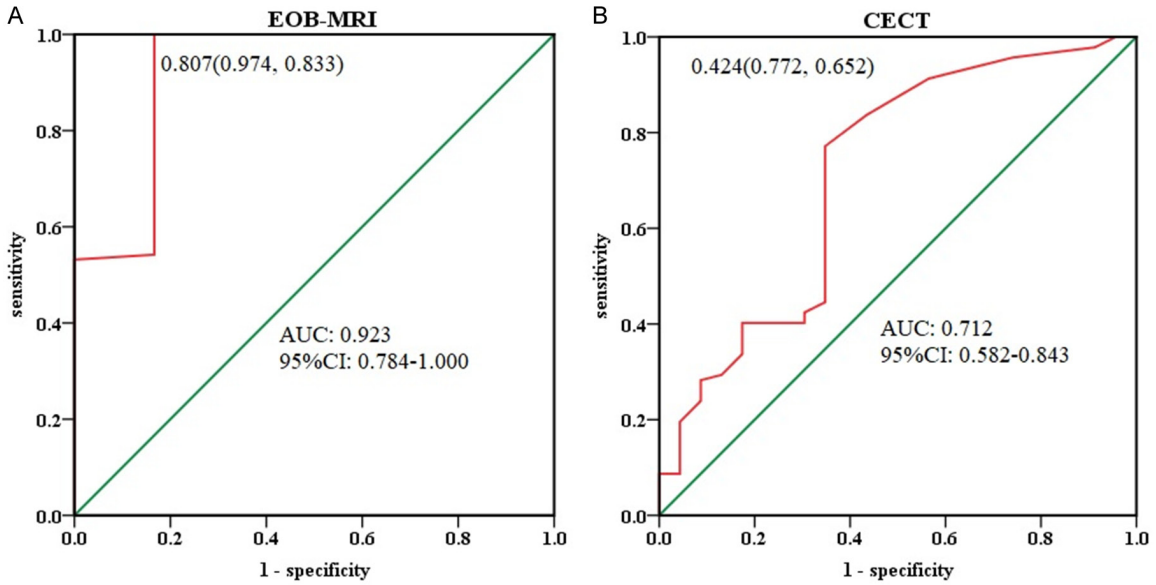

Figure 5. Receiver operator characteristic curve (ROC) of the two groups. A: Gadolinium-ethoxybenzyl-diethylene-triamine pentaacetic acid-enhanced magnetic resonance imaging (EOB-MRI); B: Contrast-enhanced computerized tomography (CECT).

Univariate analysis of each parameter of EOB-MRI for efficacy evaluation

Non-target-like enhancement in the hepatobiliary phase, non-circumferential enhancement in the arterial phase, and a difference of ≤ 2 mm in length and diameter were more frequently observed in the high-response rate group, whereas target-like enhancement in the hepatobiliary phase, circumferential enhancement in the arterial phase, and a difference of > 2 mm in length and diameter were more common in the low-response rate group, with statistically significant differences ($P < 0.05$). The ADC and NRE values were (1.4 ± 0.3) × 10^{-3} mm^2/s and (-23.7 ± 13.3) in the high-response group, and (0.9 ± 0.4) × 10^{-3} mm^2/s and (-7.1 ± 14.4) in the low-response group, with statistically significant differences between the two groups ($P < 0.05$). Additionally, statistical analysis of the length-diameter difference, Ratio M/L, CNR, and RSID revealed *P* values of 0.585, 0.926, 0.569, and 0.362, respectively (**Table 2**).

Multivariate logistic regression analysis of the parameters on the evaluation of efficacy

Logistic regression analysis was conducted with the detection of lesions after systemic treatment in early-stage hepatocellular carcinoma patients, as assessed by EOB-MRI (yes = 1, no = 0), as the dependent variable. The independent variables included parameters with statistically significant differences from the univariate analysis (hepatobiliary phase, arterial phase, length-diameter difference, ADC, and NRE), with the assigned values for these variables shown in **Table 3**. The results of the logistic regression analysis indicated that ADC and NRE could serve as independent predictors of treatment efficacy in early-stage hepatocellular carcinoma patients following systemic therapy ($P < 0.05$) (**Table 4**).

Discussion

This study retrospectively evaluated the diagnostic efficacy of EOB-MRI in early-stage hepatocellular carcinoma patients, and the findings indicated that the lesion detection rate of EOB-MRI was higher than that of CECT. Previous studies have also compared multilayer spiral CT and EOB-MRI on 130 focal liver lesions, revealing that EOB-MRI demonstrated significantly higher sensitivity, specificity, and accuracy in lesion diagnosis compared to CT. Additionally, EOB-MRI showed notable diagnostic advantages for lesions with smaller diameters [24-26], a result consistent with the present study. One possible explanation for these findings is that the signal characteristics of EOB-MRI during the hepatobiliary phase are

Table 2. Parameters of EOB-MRI [$\bar{x} \pm s$, n (%)]

Parameter	HRRG (n = 53)	LRRG (n = 47)	χ^2/t	*P*
Hepatobiliary stage			23.017	< 0.001
Target enhancement	14 (26.4)	35 (74.5)		
Off-target enhancement	39 (73.6)	12 (25.5)		
Arterial phase			19.095	< 0.001
Ring-enhancement	13 (24.5)	32 (68.1)		
Non-ring strengthening	40 (75.5)	15 (31.9)		
Length diameter difference			25.205	< 0.001
≤ 2 mm	49 (95.5)	22 (46.8)		
> 2 mm	4 (7.5)	25 (53.2)		
Hepatobiliary stage long diameter			0.298	0.585
≤ 20 mm	22 (41.5)	17 (36.2)		
> 20 mm	31 (58.5)	30 (63.8)		
ADC ($\times 10^{-3}$ mm^2/s)	1.4 ± 0.3	0.9 ± 0.4	-7.622	< 0.001
Ratio M/L	0.5 ± 0.2	0.5 ± 0.2	-0.093	0.926
NRE	-23.7 ± 13.3	-7.1 ± 14.4	5.994	< 0.001
CNR	-21.2 ± 2.4	-21.0 ± 2.1	0.571	0.569
RSID	491.5 ± 98.8	473.3 ± 99.4	-0.915	0.362

Note: EOB-MRI: Gadolinium-ethoxybenzyl-diethylenetriamine pentaacetic acid-enhanced magnetic resonance imaging; HRRG: high response rate group; LRRG: low response rate group; ADC: apparent diffusion coefficient; NRE: normalized relative enhancement; CNR: contrast-to-noise ratio; RSID: relative signal intensity difference.

Table 3. Assignment table of argument variables

Independent variable	Value
Hepatobiliary stage	Target enhancement = 1; off-target enhancement = 0
Arterial phase	Ring-enhancement = 1; non-ring strengthening = 0
Length diameter difference	≤ 2 mm = 1; > 2 mm = 0
ADC	Original input
NRE	Original input

Note: ADC: apparent diffusion coefficient; NRE: normalized relative enhancement.

Table 4. Logistic regression analysis of factors affecting the outcome of patients with early-stage hepatocellular carcinoma after systemic therapy

Variate	Regression coefficient	Standard error	Wald χ^2	*P*	OR	95% CI	
						Lower limit	Upper limit
Constant	-18.184	7.887	5.315	0.021	-	-	-
Hepatobiliary stage	17.642	3812.623	0.000	0.996	45888810.30	-	-
Arterial phase	9.667	3832.271	0.000	0.998	15783.438	-	-
Length diameter difference	-29.216	5392.254	0.000	0.996	0.000	-	-
ADC	6.755	2.593	6.788	0.009	858.191	5.330	138180.955
NRE	-0.135	0.047	8.238	0.004	0.873	0.796	0.958

Note: ADC: apparent diffusion coefficient; NRE: normalized relative enhancement; OR: odds ratio; CI: confidence interval.

related to liver cell function. Most focal liver lesions, such as hepatic hemangioma, hepatic cysts, hepatocellular carcinoma, and cholangiocarcinoma, either lack liver cells or do not contain functional liver cells, preventing the uptake of Gd-EOB-DTPA. Consequently, in hepatobiliary phase imaging, these lesions exhibit low signals, in contrast to the normal liver parenchyma, thereby enhancing the signal contrast between the lesion and surround-

ing tissue and facilitating lesion detection [27, 28].

However, hepatic lesions do not always exhibit a true "uptake deficit". Studies have shown that between 8.8% and 46.7% of liver lesions display target-like enhancement in the hepatobiliary phase, which may be due to contrast retention caused by connective tissue proliferation [29-31]. Additionally, circumferential enhancement of lesions in the arterial phase may result from either enhancement of the tumor itself or enhancement of the peritumoral hepatic parenchyma. The latter is typically associated with histopathological features such as peritumoral connective tissue proliferation, inflammatory cell infiltration, and vascular proliferation [32]. Notably, tumors showing target-like enhancement in the hepatobiliary phase often contain significant amounts of fibrous connective tissue and tumor-associated fibroblasts, which may confer resistance to anticancer drugs, leading to poorer treatment outcomes. Literature has reported that target-like enhancement in the hepatobiliary phase of liver metastases from breast cancer is predictive of poor chemotherapy efficacy and shorter survival [33, 34]. Furthermore, the presence or absence of peritumoral hepatic parenchyma enhancement in the arterial phase has been linked to the assessment of treatment efficacy in colorectal cancer liver metastases. Chun et al. proposed a set of morphological evaluation criteria based on CT-enhanced scans, indicating that features such as uneven tumor density, a blurred tumor-hepatic interface, and a thicker peritumoral enhancement ring in the arterial phase are closely associated with poor treatment response [35]. In this study, while the ratio of target-like to non-target-like enhancement in the hepatobiliary phase and the difference in longitudinal diameter between the arterial and hepatobiliary phases showed statistically significant differences in univariate analysis, they did not emerge as independent predictors of response rate after logistic regression. Therefore, the role of target-like enhancement in predicting the efficacy of systemic therapy for early-stage hepatocellular carcinoma warrants further investigation.

After multivariate analysis, the ADC and NRE values were found to be statistically different between the high and low response rate groups in this study and were identified as independent predictors of efficacy in early-stage hepatocellular carcinoma patients. Kubota et al. demonstrated that ADC could be effectively used to assess the treatment response in hepatocellular carcinoma patients following transcatheter arterial chemoembolization [36, 37]. This is likely due to the fact that ADC values are closely associated with factors such as molecular viscosity, membrane permeability, active transport mechanisms, microvascular circulation, and the directional movement of tissues and cellular structures. As a result, ADC can be utilized to evaluate treatment response and cellular changes after therapy. Following effective treatment, there is a decrease in cell density, lessened hindrance to water molecule movement, and an increase in tumor ADC values, which explains why the high response rate group had higher ADC values compared to the low response rate group [38, 39]. NRE, on the other hand, reflects the degree of contrast retention in the delayed phase, which appears as delayed enhancement in dynamic imaging. Additionally, angiogenesis may be suppressed in tumors that respond well to treatment, leading to a reduced change in signal intensity after contrast enhancement.

Conclusion

EOB-MRI demonstrates superior detection efficacy for early liver lesions, and parameters such as ADC and NRE can serve as independent predictors for evaluating the treatment outcomes of early-stage hepatocellular carcinoma patients. However, this study has several limitations. While EOB-MRI shows high sensitivity in detecting small hepatocellular carcinoma lesions, its detection capability still needs further improvement, particularly for exceptionally small lesions. Additionally, the literature lacks information on the correlation between lesion response rates after systemic treatment and patient prognosis or survival. As a result, the median response rate was used as the cut-off to distinguish between the high and low response rate groups, which may introduce bias due to the limited sample size. The functional status of background hepatocytes also impacts the degree of Gd-EOB-DTPA uptake, thereby affecting the accuracy of quantitative parameters. To enhance the application of EOB-MRI in diagnosing, assessing treatment efficacy, and predicting prognosis in early-stage hepatocel-

lular carcinoma patients, further studies are needed to identify more effective methods.

Acknowledgements

This work was supported by Open Funding Project of Jiangsu Key Laboratory of Encephalopathy Bioinformatics (XZSYSKF2023026).

Disclosure of conflict of interest

None.

Address correspondence to: Liang-Qing Liu, Department of Imaging, Wujin Clinical College of Xuzhou Medical University, No. 2 Yongning North Road, Tianning District, Changzhou 213002, Jiangsu, China. Tel: +86-0519-85579706; E-mail: llq19832024@163.com

References

[1] Crane H, Gofton C, Sharma A and George J. MAFLD: an optimal framework for understanding liver cancer phenotypes. J Gastroenterol 2023; 58: 947-964.

[2] Wang ZG, He ZY, Chen YY, Gao H and Du XL. Incidence and survival outcomes of secondary liver cancer: a surveillance epidemiology and end results database analysis. Transl Cancer Res 2021; 10: 1273-1283.

[3] Li Q, Cao M, Lei L, Yang F, Li H, Yan X, He S, Zhang S, Teng Y, Xia C and Chen W. Burden of liver cancer: from epidemiology to prevention. Chin J Cancer Res 2022; 34: 554-566.

[4] Cho Y, Kim BH and Park JW. Overview of Asian clinical practice guidelines for the management of hepatocellular carcinoma: an Asian perspective comparison. Clin Mol Hepatol 2023; 29: 252-262.

[5] Lampimukhi M, Qassim T, Venu R, Pakhala N, Mylavarapu S, Perera T, Sathar BS and Nair A. A review of incidence and related risk factors in the development of hepatocellular carcinoma. Cureus 2023; 15: e49429.

[6] Park JW, Chen M, Colombo M, Roberts LR, Schwartz M, Chen PJ, Kudo M, Johnson P, Wagner S, Orsini LS and Sherman M. Global patterns of hepatocellular carcinoma management from diagnosis to death: the BRIDGE study. Liver Int 2015; 35: 2155-2166.

[7] Yu XC, Liu JB, Tang QH, Diao X, Fan QY, Huang ZY, Tang XM, Li S, Cao YF, Ma YS and Fu D. Recent trends in the incidence and survival of stage I liver cancer: a surveillance, epidemiology, and end results analysis. Ann Med 2022; 54: 2785-2795.

[8] Sangiovanni A and Colombo M. Treatment of hepatocellular carcinoma: beyond international guidelines. Liver Int 2016; 36 Suppl 1: 124-129.

[9] Tümen D, Heumann P, Gülow K, Demirci CN, Cosma LS, Müller M and Kandulski A. Pathogenesis and current treatment strategies of hepatocellular carcinoma. Biomedicines 2022; 10: 3202.

[10] Zhang J, Feng GA, Li Y and Wang W. Drug-eluting bead transarterial chemoembolization with medium-sized versus small-sized CalliSpheres microspheres in unresectable primary liver cancer. Asia Pac J Clin Oncol 2022; 18: 388-393.

[11] Liu Y, Wu D, Zhang K, Ren R, Liu Y, Zhang S, Zhang X, Cheng J, Chen L and Huang J. Detection technology and clinical applications of serum viral products of hepatitis B virus infection. Front Cell Infect Microbiol 2024; 14: 1402001.

[12] Selzner M, Hany TF, Wildbrett P, McCormack L, Kadry Z and Clavien PA. Does the novel PET/CT imaging modality impact on the treatment of patients with metastatic colorectal cancer of the liver? Ann Surg 2004; 240: 1027-1034; discussion 1035-1036.

[13] Tanaka S, Sato N, Fujioka H, Takahashi Y, Kimura K, Iwamoto M and Uchiyama K. Use of contrast-enhanced computed tomography in clinical staging of asymptomatic breast cancer patients to detect asymptomatic distant metastases. Oncol Lett 2012; 3: 772-776.

[14] Zhang W, Kong X, Wang ZJ, Luo S, Huang W and Zhang LJ. Dynamic contrast-enhanced magnetic resonance imaging with Gd-EOB-DTPA for the evaluation of liver fibrosis induced by carbon tetrachloride in rats. PLoS One 2015; 10: e0129621.

[15] Li X, Jing H, Cheng L, Xia J, Wang J, Li Q, Liu C and Cai P. A case study of glycogen storage disease type Ia presenting with multiple hepatocellular adenomas: an analysis by gadolinium ethoxybenzyl-diethylenetriamine-pentaacetic acid magnetic resonance imaging. Quant Imaging Med Surg 2021; 11: 2785-2791.

[16] Minamiguchi K, Marugami N, Uchiyama T, Kusano H, Yasuda S, Sho M and Tanaka T. Imaging features of β-catenin-activated hepatocellular adenoma with weak β-catenin activation: a rare case report. Acta Radiol Open 2022; 11: 20584601221142241.

[17] Takenaga T, Hanaoka S, Nomura Y, Nakao T, Shibata H, Miki S, Yoshikawa T, Hayashi N and Abe O. Multichannel three-dimensional fully convolutional residual network-based focal liver lesion detection and classification in Gd-EOB-DTPA-enhanced MRI. Int J Comput Assist Radiol Surg 2021; 16: 1527-1536.

[18] Takakusagi S, Yokoyama Y, Kizawa K, Marubashi K, Kosone T, Sato K, Kakizaki S, Harada K, Takagi H and Uraoka T. Successfully treated case of cholangiolocellular carcinoma with a poor hepatic functional reserve reporting with various imaging findings. Intern Med 2021; 60: 873-881.
[19] Chen JP, Yang RH, Zhang TH, Liao LA, Guan YT and Dai HY. Pre-operative enhanced magnetic resonance imaging combined with clinical features predict early recurrence of hepatocellular carcinoma after radical resection. World J Gastrointest Oncol 2024; 16: 1192-1203.
[20] Omata M, Cheng AL, Kokudo N, Kudo M, Lee JM, Jia J, Tateishi R, Han KH, Chawla YK, Shiina S, Jafri W, Payawal DA, Ohki T, Ogasawara S, Chen PJ, Lesmana CRA, Lesmana LA, Gani RA, Obi S, Dokmeci AK and Sarin SK. Asia-Pacific clinical practice guidelines on the management of hepatocellular carcinoma: a 2017 update. Hepatol Int 2017; 11: 317-370.
[21] Korean Liver Cancer Association; National Cancer Center. 2018 Korean Liver Cancer Association-National Cancer Center Korea practice guidelines for the management of hepatocellular carcinoma. Gut Liver 2019; 13: 227-299.
[22] Shan T, Ran X, Li H, Feng G, Zhang S, Zhang X, Zhang L, Lu L, An L, Fu R, Sun K, Wang S, Chen R, Li L, Chen W, Wei W, Zeng H and He J. Disparities in stage at diagnosis for liver cancer in China. J Natl Cancer Cent 2023; 3: 7-13.
[23] Zhong BY, Jiang JQ, Sun JH, Huang JT, Wang WD, Wang Q, Ding WB, Zhu XL and Ni CF. Prognostic performance of the china liver cancer staging system in hepatocellular carcinoma following transarterial chemoembolization. J Clin Transl Hepatol 2023; 11: 1321-1328.
[24] Böttcher J, Hansch A, Pfeil A, Schmidt P, Malich A, Schneeweiss A, Maurer MH, Streitparth F, Teichgräber UK and Renz DM. Detection and classification of different liver lesions: comparison of Gd-EOB-DTPA-enhanced MRI versus multiphasic spiral CT in a clinical single centre investigation. Eur J Radiol 2013; 82: 1860-1869.
[25] Wang F, Numata K, Okada M, Chuma M, Nihonmatsu H, Moriya S, Nozaki A, Ogushi K, Luo W, Ruan L, Nakano M, Otani M, Inayama Y and Maeda S. Comparison of Sonazoid contrast-enhanced ultrasound and gadolinium-ethoxybenzyl-diethylenetriamine pentaacetic acid MRI for the histological diagnosis of hepatocellular carcinoma. Quant Imaging Med Surg 2021; 11: 2521-2540.
[26] Qing Z, Yuan H, Hao X and Jie P. Diagnostic value of CT delayed phase images added to Gd-EOB-DTPA MRI for HCC diagnosis in LR-3/4 lesions. Int J Gen Med 2023; 16: 2383-2391.
[27] Semaan S, Vietti Violi N, Lewis S, Chatterji M, Song C, Besa C, Babb JS, Fiel MI, Schwartz M, Thung S, Sirlin CB and Taouli B. Hepatocellular carcinoma detection in liver cirrhosis: diagnostic performance of contrast-enhanced CT vs. MRI with extracellular contrast vs. gadoxetic acid. Eur Radiol 2020; 30: 1020-1030.
[28] Qin Z, Zhou Y, Zhang X, Ding J, Zhou H, Wang Y, Zhao L, Chen C and Jing X. The comparison of contrast-enhanced ultrasound and gadoxetate disodium-enhanced MRI LI-RADS for nodules ≤ 2 cm in patients at high risk for HCC: a prospective study. Front Oncol 2024; 14: 1345981.
[29] Granata V, Catalano O, Fusco R, Tatangelo F, Rega D, Nasti G, Avallone A, Piccirillo M, Izzo F and Petrillo A. The target sign in colorectal liver metastases: an atypical Gd-EOB-DTPA "uptake" on the hepatobiliary phase of MR imaging. Abdom Imaging 2015; 40: 2364-2371.
[30] Seth A, Amemiya Y, Cheung H, Hsieh E, Law C and Milot L. Delayed MRI enhancement of colorectal cancer liver metastases is associated with metastatic mutational profile. Cancer Genomics Proteomics 2021; 18: 627-635.
[31] Zhou C, Liu Q, Meng F, Ding N, Yan J and Liu B. Modification of erythrocytes by internalizing Arg-Gly-Asp (iRGD) in boosting the curative effect of radiotherapy for gastric carcinoma. J Gastrointest Oncol 2022; 13: 2249-2258.
[32] Semelka RC, Hussain SM, Marcos HB and Woosley JT. Perilesional enhancement of hepatic metastases: correlation between MR imaging and histopathologic findings-initial observations. Radiology 2000; 215: 89-94.
[33] Lee HJ, Lee CH, Kim JW, Park YS, Lee J and Kim KA. Use of hepatobiliary phase images in Gd-EOB-DTPA-enhanced MRI of breast cancer hepatic metastasis to predict response to chemotherapy. Clin Imaging 2017; 43: 127-131.
[34] Brunskill N, Robinson J, Nocum D and Reed W. Exploring software navigation tools for liver tumour angiography: a scoping review. J Med Radiat Sci 2024; 71: 261-268.
[35] Hosokawa A, Yamazaki K, Matsuda C, Ueda S, Kusaba H, Okamura S, Tsuda M, Tamura T, Shinozaki K, Tsushima T, Tsuda T, Shirakawa T, Yamashita H, Morita S, Hironaka S and Muro K. Morphologic response to chemotherapy containing bevacizumab in patients with colorectal liver metastases: a post hoc analysis of the WJOG4407G phase III study. Medicine (Baltimore) 2020; 99: e22060.
[36] Kubota K, Yamanishi T, Itoh S, Murata Y, Miyatake K, Yasunami H, Morio K, Hamada N, Nishioka A and Ogawa Y. Role of diffusion-weighted imaging in evaluating therapeutic efficacy after transcatheter arterial chemoembolization for hepatocellular carcinoma. Oncol Rep 2010; 24: 727-32.

[37] Thormann M, Heitmann F, Wrobel V, March C, Pech M, Surov A, Damm R and Omari J. Interstitial brachytherapy of the liver for renal cell carcinoma: ADC measurements do not predict overall survival. In Vivo 2022; 36: 2945-2951.
[38] Liu LH, Zhou GF, Lv H, Wang ZC, Rao SX and Zeng MS. Identifying response in colorectal liver metastases treated with bevacizumab: development of RECIST by combining contrast-enhanced and diffusion-weighted MRI. Eur Radiol 2021; 31: 5640-5649.
[39] Hosseini-Nik H, Fischer SE, Moulton CA, Karbhase G, Menezes RJ, Gallinger S and Jhaveri KS. Diffusion-weighted and hepatobiliary phase gadoxetic acid-enhanced quantitative MR imaging for identification of complete pathologic response in colorectal liver metastases after preoperative chemotherapy. Abdom Radiol (NY) 2016; 41: 231-238.